Flinders
UNIVERSITY

DOI: 10.1039/B813359J

Dryza, V., Gascooke, J.R., Buntine, M.A., & Metha, G.F., 2009. Onset of carbon-carbon bonding in the Nb5Cy (y = 0-6) clusters : a threshold photo-ionisation and density functional theory study. Physical Chemistry Chemical Physics, 11(7), 1060-1068.

Onset of carbon–carbon bonding in the Nb_5C_y (y = 0–6) clusters: a threshold photo-ionisation and density functional theory study†

Viktoras Dryza, Jason R. Gascooke,‡ Mark. A. Buntine and Gregory F. Metha*

Received 4th August 2008, Accepted 20th October 2008
First published as an Advance Article on the web 18th December 2008
DOI: 10.1039/b813359j

We have used photo-ionisation efficiency spectroscopy to determine the ionisation potentials (IPs) of the niobium–carbide clusters, Nb_5C_y (y = 0–6). Of these clusters Nb_5C_2 and Nb_5C_3 exhibit the lowest IPs. Complementary density functional theory calculations have been performed to locate the lowest energy isomers for each cluster. By comparing the experimental IPs with those calculated for candidate isomers, the structures of the Nb_5C_y clusters observed in the experiment are inferred. For all these structures, the underlying Nb_5 cluster has either a "prolate" or "oblate" trigonal bipyramid geometry. Both Nb_5C_5 and Nb_5C_6 are shown to contain carbon–carbon bonding in the form of one and two molecular C_2 units, respectively.

I. Introduction

Metal–carbide clusters have been proposed for applications in nanotechnology such as molecular wires,[1] nanocatalysis[2–5] and hydrogen storage.[6,7] Knowledge of the structures of metal–carbide clusters is important in understanding their potential applications. Despite this, many metal–carbide clusters still have unknown structures.

Previous studies on metal–carbide clusters have shown that their structures can be inferred by the determination of their experimental ionisation potentials (IPs) or electron affinities (EAs), in combination with density functional theory (DFT) calculations on candidate isomers.[8–15] Since different structural isomers will generally have different ionisation energies, determination of this property helps to guide the search for the lowest energy isomer by either including or excluding potential candidates.

The growth patterns of metal–carbide clusters towards larger clusters and the onset of certain structural motifs, such as carbon–carbon bonding found in Met-cars (M_8C_{12}), are also important.[1,9,15–19] For example, Castleman and co-workers have recently investigated the structures of anionic Nb_2C_y clusters by a combined photoelectron spectroscopy and DFT study.[15] In particular, they noted that Nb_2C_5 and Nb_2C_6 have 3D structures, yet Nb_2C_7 has a linear structure where a niobium atom is attached to either end of a carbon chain.

Photo-dissociation experiments on cationic niobium–carbide clusters have been performed by Duncan and co-workers.[20] In the size range of interest in this study, they found $Nb_5C_3^+$ to be a prominent species in the nascent distribution from the ablation source. However, $Nb_5C_3^+$ was not observed to be an abundant photo-dissociation product of larger clusters. It was proposed that Nb_5C_3 had a substituted 2 × 2 × 2 cubic structure, where one carbon atom in a 2 × 2 × 2 face-centred cubic (fcc) Nb_4C_4 nanocrystal is replaced with a niobium atom.

The species Nb_3C_2 and Nb_5C_2 have previously been investigated by PFI-ZEKE photoelectron spectroscopy, with their IPs determined to be 5.04 and 4.60 eV, respectively.[21,22] The PFI-ZEKE spectrum of Nb_3C_2 displayed a relatively long vibronic progression. Conversely, the spectrum of Nb_5C_2 only displayed the 0–0 transition and a small number of sequence bands. While a trigonal bipyramid geometry possessing separated carbon atoms was assigned to the spectrum of Nb_3C_2, no calculations on the structure of Nb_5C_2 were performed.

Using a tuneable IR-free electron laser (IR-FEL), Meijer, von Helden and co-workers have collected IR-resonance enhanced multiphoton ionisation (IR-REMPI) spectra for various niobium–carbide clusters.[23] Single broad absorption resonances were observed for Nb_4C_4 and Nb_5C_3, centred at 675 and 660 cm^{-1}, respectively. The observed resonances are similar to one of two IR-active phonon modes of the metallic NbC (100) surface[24] and are direct evidence of the proposed nanocystalline structure of Nb_4C_4. For Nb_5C_3 the resonance is similar to Nb_4C_4, indicating that the proposed structure of a substituted nanocrystal is quite plausible for the former species.

In this study, we present photo-ionisation efficiency (PIE) data for the pentaniobium–carbide clusters. Structures for the clusters are inferred by comparison between the extracted IPs and those calculated for the lowest energy DFT isomers. It is shown that the structure of the underlying Nb_5 cluster has two competing geometries in these niobium–carbide clusters. Additionally, carbon–carbon bonding (in the form of C_2 units) is present in the structures assigned to the ionisation onsets of Nb_5C_5 and Nb_5C_6.

Department of Chemistry, The University of Adelaide, South Australia, 5005 Australia. E-mail: greg.metha@adelaide.edu.au; Fax: +61 8 8303 4358; Tel: +61 8 8303 5943

† Electronic supplementary information (ESI) available: Electronic state, structural symmetry, absolute energies (B3P86/Nb SDD, C aug-cc-pVTZ) and relative energies (excluding zero point energies) for the neutral and cationic niobium-carbide cluster isomers. See DOI: 10.1039/b813359j

‡ Present address: School of Chemistry, Physics and Earth Sciences, The Flinders University of South Australia, Bedford Park, SA 5042, Australia

II. Experimental and computational methods

A Experimental

The experimental details of the laser ionisation experiments are similar to those reported previously.[8,9] Briefly, niobium–carbide clusters are formed in a supersonic laser ablation source coupled to a time-of-flight mass spectrometer (TOF-MS). A gas mix consisting of 0.02% acetylene seeded in helium is reacted with the ablation products of a niobium rod and passed along a 15 mm long "condensation tube" before undergoing expansion into the first vacuum chamber. The clusters pass *via* a homebuilt skimmer into the second chamber that contains a standard Wiley-McLaren TOF-MS arranged perpendicularly with the cluster molecular beam. The neutral clusters are ionised with the frequency-doubled output of a Nd:YAG-pumped dye laser. All data points are collected at 0.2 nm intervals. The resultant ions are detected by a double multi-channel plate detector, amplified ×25 (Stanford SR445) and the signal sent to a digital oscilloscope (LeCroy 9350 AM, 500 MHz) for averaging (1000 laser shots) before being saved on a PC for analysis. Typical laser powers used are 50 μJ/pulse, collimated to a 5 mm diameter beam, as measured using a power meter (Ophir PE10BB). Under these conditions, all ion signals are found to be linearly dependent with laser fluence. During each PIE scan, the laser power is kept constant. To check that long term intensity fluctuations in the cluster source had not occurred, the laser is returned to the starting wavelength immediately after each scan to ensure that the cluster signal intensity had remained constant.

B Computational

Geometry optimisation and harmonic vibrational frequency calculations were performed using DFT in the Gaussian 03 suite of programs.[25] Initial calculations were made using the B3P86 method with the SDD basis set to locate a range of geometric isomers for each neutral cluster species at the two lowest spin multiplicities (*i.e.* doublet and quartet) using a range of starting geometries. Subsequently, all low-lying isomers (typically within 0.7 eV of a global minimum), were re-calculated using the aug-cc-pVTZ basis set on the carbon atoms in an effort to improve the treatment of these atoms which is herein referred to as the "extended" basis set. For both basis sets, all isomers were initially optimised without any geometry constraint. The minimised isomers were then examined to determine any symmetry properties and the calculations were repeated within the highest symmetry point group. The symmetry-constrained energy was subsequently compared to the unconstrained energy to ensure that there was no difference. All isomers were characterised with vibrational frequency calculations to determine whether the optimised structure is a true minimum. All reported isomers, relative energetics, ionisation potentials and molecular symmetries (including term symbols) were obtained using the extended basis set. All of the isomers identified using only the SDD basis set are presented in the ESI.†

For all the geometries presented herein (and in the ESI†), bonds are drawn between niobium atoms if their distance is less than, or equal to, twice the covalent radius (*i.e.* $\leq$ 2.74 Å). Niobium-carbon bonds are drawn at bond lengths $\leq$ 2.35 Å. This distance is longer than the covalent radius of the niobium and carbon atoms combined (2.14 Å) to signify the importance of niobium-carbon bonding and back-bonding effects for isomers with C_2 units. Carbon-carbon bonds are drawn as follows; 1.60 Å > single bond > 1.40 Å > double bond > 1.25 Å > triple bond. Atomic charges were determined by Natural Bond Order calculations.[26]

III. Results and discussion

A Mass spectra and photo-ionisation efficiency spectra

The mass spectrum of neutral niobium–carbide clusters obtained by single photon ionisation at 225 nm (5.51 eV) is shown in Fig. 1. As can be seen in the expanded Nb_5C_y region, the Nb_5 cluster appears with 1–6 C atoms attached. This distribution did not change up to the highest available photon energy in our laboratory (210 nm, 5.91 eV). It is observed that the majority of the Nb_5C_y peaks display shoulders to the higher mass side. These shoulders are believed to be Nb_5C_yO species, due to an oxide layer present on the Nb rod, rather than $Nb_5C_yH_2$ species, due to incomplete dehydrogenation of the acetylene precursor. Indeed, experiments in a low pressure pickup cell have shown that total dehydrogenation occurs for the first three C_2H_2 molecules attached to the neutral Nb_5 cluster.[27]

PIE spectra are recorded by monitoring the signal of each species as a function of photon energy. The shoulders present on the peaks due to oxide contamination were not included in the integration. PIE spectra for the Nb_5C_y (y = 0–6) clusters are shown in parts a–g of Fig. 2. The clusters Nb_5C_2, Nb_5C_3 and Nb_5C_6 show a dramatic rise from the baseline indicating good Frank-Condon overlap between the ground electronic states of the neutral and cation. Conversely, the clusters Nb_5C, Nb_5C_4 and Nb_5C_5 show gradual onsets of ionisation, suggesting some geometry change between the neutral and cation. For all spectra two lines are fitted; one to the baseline and one to the linear rise of signal, and their intersection defined as the IP. This method provides a determination of the IP with an estimated error of ±0.05 eV. Although the ionisation process is vertical, as little geometry change is observed between the neutral and cationic ground states for larger clusters, the onsets of ionisation will be good approximations to the adiabatic IPs. The

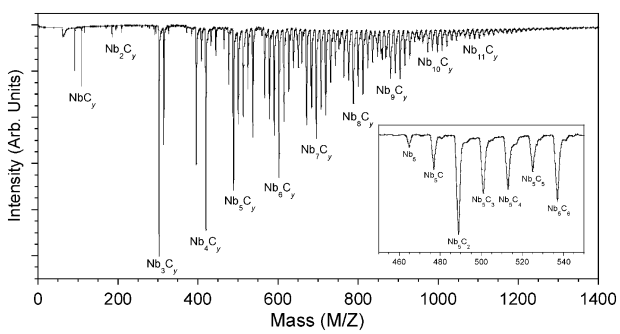

Fig. 1 Mass spectrum of neutral Nb_xC_y clusters obtained by single-photon ionisation at 225 nm. The inset shows an expanded view of the Nb_5C_y region.

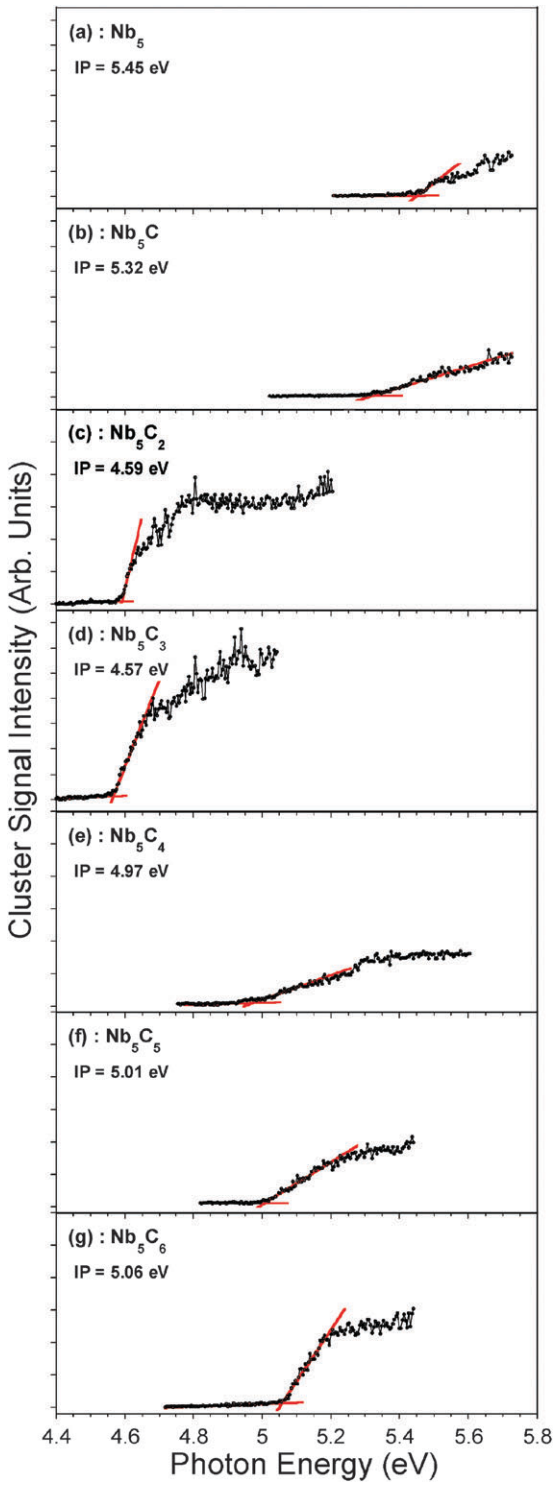

Fig. 2 Photo-ionisation efficiency spectra for Nb_5C_y (y = 0–6) clusters. The determined IPs are also listed.

determined IPs are given in the PIE spectra and will be also presented later. As a check, the IPs extracted for Nb_5 and Nb_5C_2 are found to be in good agreement with those previously determined.[22,28,29]

For the Nb_5C_y series, relative to the IP of Nb_5, addition of one C atom to Nb_5 only slightly reduces the IP (−0.13 eV). However, addition of two and three C atoms cause significant IP reductions of −0.86 and −0.88 eV, respectively. Addition of four, five and six C atoms to Nb_5 all cause similar intermediate IP reductions of −0.48, −0.44 and −0.39 eV, respectively.

B DFT calculated Nb_5C_y isomers

All the calculated isomers considered for the *neutral* Nb_5C_y (y = 0–3) and Nb_5C_y (y = 4–6) clusters are shown in Fig. 3 and 4, respectively. The relative energies (eV, excluding zero-point energy correction) for each isomer of the neutral species are also shown. For each isomer, similar geometric minima are also identified on the *cationic* surface, however, these are not included in the figures but the information appears in the ESI.† Almost all discussion herein refers to the neutral systems but reference is made to the cationic systems when results can be compared with previous studies. All details (*i.e.* geometric and energy information) for both neutral and cationic isomers is contained in the ESI.†

The structure of the neutral and cationic niobium pentamer have previously been investigated by Majumdar and Balasubramanian with the DFT and multi-reference configuration-interaction (MR-CI) methods.[30,31] For the DFT method a distorted trigonal bipyramid geometry was found for Nb_5 [$^2A_2$, C_{2v}], whereas for Nb_5^+ a distorted trigonal bipyramid of high spin multiplicity [$^3A_1$, C_{2v}] was found. In this study the lowest energy structure of Nb_5 is also found to be a distorted prolate trigonal bipyramid, **I A** [$^2B_1$, C_{2v}]. This electronic state is different than that of Majumdar and Balasubramanian with the DFT method, however it is the same as that obtained with the MR-CI method. The lowest energy structure of the cation, **I A**$^+$ [$^3A_1$, C_{2v}], is found to agree with the previous work. Recent IR multi-photon dissociation (IR-MPD) experiments

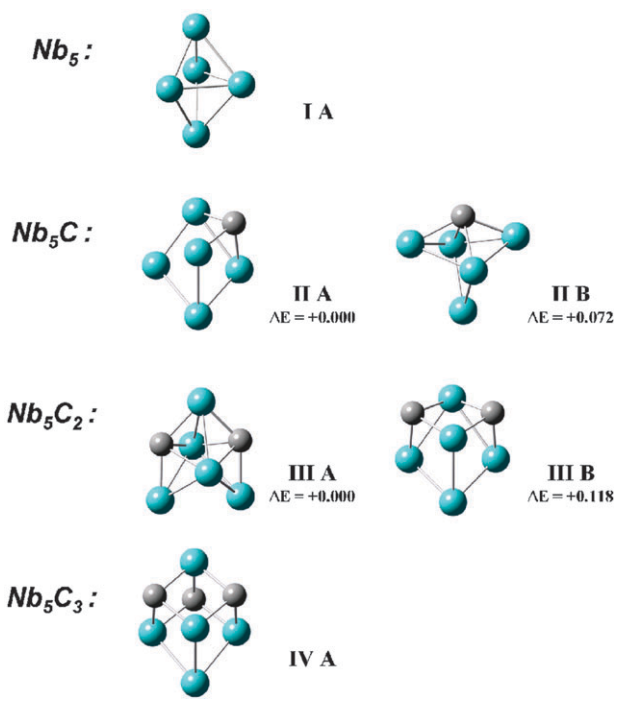

Fig. 3 Structures of the calculated isomers for the neutral Nb_5C_y (y = 0–3) clusters. Written beneath each isomer are the relative energies (ΔE in eV) calculated using the extended basis sets.

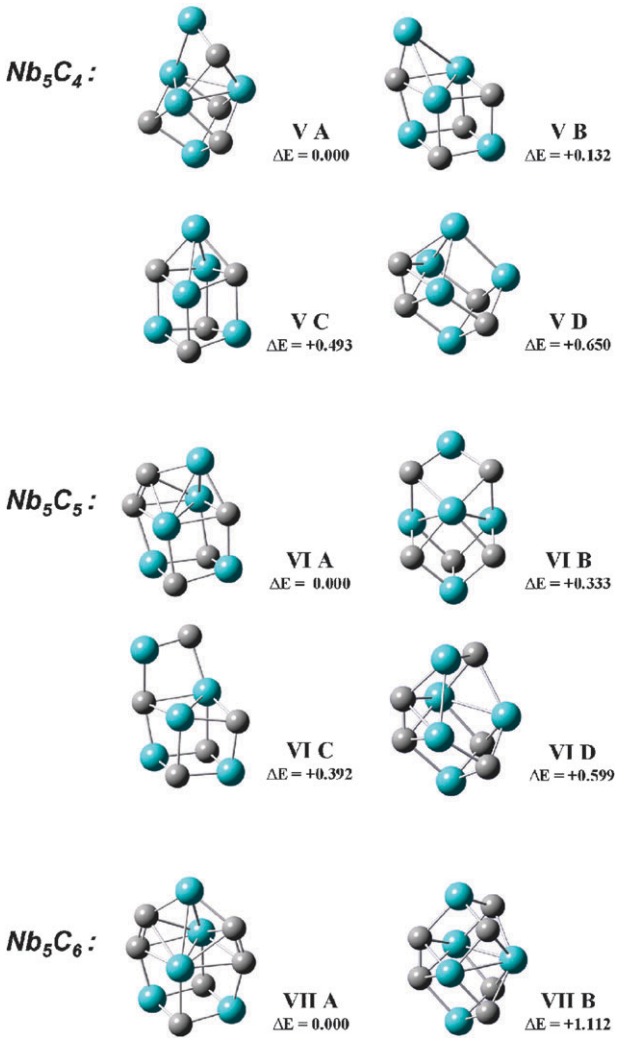

Fig. 4 Structures of the calculated isomers for the neutral Nb_5C_y (y = 4–6) clusters. Written beneath each isomer are the relative energies (ΔE in eV) calculated using the extended basis sets.

with an IR-FEL on Nb_5-Ar and Nb_5^+-Ar are consistent with these calculated results.[32]

Before the isomeric structures of the Nb_5C_y clusters are discussed, it is useful to describe the geometries the underlying Nb_5 motif may have in these clusters. Analogous to the lowest energy Nb_5 structure there is the prolate "trigonal bipyramid" geometry where the two axial Nb atoms are at a longer distance to the centre of mass than the three equatorial Nb atoms. There may also be an "oblate trigonal bipyramid" geometry, where the two axial Nb atoms are at a shorter distance to the centre of mass than the three equatorial Nb atoms. Both of these are shown in Fig. 5. This latter geometry is not favourable for the bare Nb_5 cluster as the three equatorial Nb atoms are not within a reasonable bonding distance of each other.[30] However, this structure is beneficial for the Nb_5C_y clusters as it creates three Nb "butterfly motifs". This is shown in the middle structure of Fig. 5 where the two axial atoms labelled A can form 3 identical "butterflies" with two of the equatorial atoms labelled E. However, as will be shown below, it is not energetically favourable for

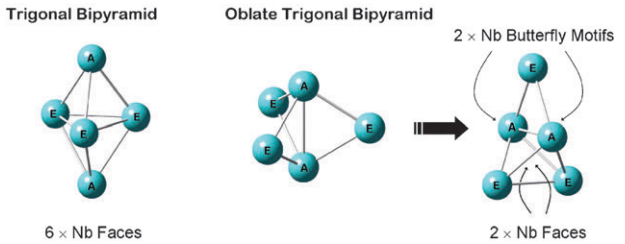

Fig. 5 The two common underlying Nb_5 geometries contained in the Nb_5C_y isomers; *i.e.* the trigonal bipyramid and oblate trigonal bipyramid geometries. The "A" and "E" labels refer to axial and equatorial atoms, respectively. The type and number of carbon addition sites for each Nb_5 geometry are also given.

C atoms or units to bind across all three Nb butterfly motifs. Rather this oblate trigonal bipyramid geometry distorts significantly once two Nb butterfly motifs have C atoms or units bound across them, with the third becoming quite closed and instead creates two outer Nb faces for C atoms to bind to. Harris and Dance have previously noted that Nb butterfly motifs which have C_2 units bound across them are energetically favourable when incorporated into the structures of larger niobium–carbide clusters.[33] From a simple valence bond perspective, a C_2 unit bonding across a Nb butterfly motif can be considered as an acetylide (C_2^{2-}) unit undergoing two σ-interactions with two equatorial Nb atoms (*i.e.* two 2-centre 2-electron bonds) and two side-on π-interactions with the other two axial Nb atoms (*i.e.* two 3-centre 2-electron bonds).

In general, the trigonal bipyramid Nb_5 cluster has six Nb faces available for C addition. The situation where C atoms bind to these Nb faces is interesting as at least two structural isomers are possible for the Nb_5C_y (y = 2–4) clusters. This is different to the case for the Nb_4C_y clusters where after each C atom is bound to a Nb face of the tetrahedral Nb_4 cluster, the remaining faces are essentially equivalent for binding of the next C atom. Alternatively, the oblate trigonal bipyramid Nb_5 cluster has two Nb butterfly motifs and two outer Nb faces available for C addition.

Two isomers are found for Nb_5C; one with the C atom bound to a Nb face of the trigonal bipyramid Nb_5 cluster, **II A** [^2A, C_1], while the other has the C atom bound across a Nb butterfly motif of the oblate trigonal bipyramid Nb_5 cluster, **II B** [$^2A_1$, C_{2v}]. Isomer **II A** is found to be the lowest in energy, although **II B** is negligibly higher in energy (ΔE = +0.072 eV). Several structures attempted with Nb–Nb edge bound C atoms are either transition states or unstable, with optimisation leading to **II A**.

The structure of Nb_5C_2 has previously been investigated by Parnis and co-workers.[34] They found the lowest energy isomer to have the two C atoms bound to separate Nb faces of the trigonal bipyramid Nb_5 cluster. In the present study the lowest energy isomer **III A** [$^2B_1$, C_{2v}] has the C atoms bound across the two Nb butterfly motifs of the oblate trigonal bipyramid Nb_5 cluster. Isomer **III B** [$^2A'$, C_s] is that identified by Parnis and is only 0.118 eV higher in energy. **III B** has C atoms bound to Nb faces next to each other that share a common axial Nb atom.

Harris and Dance have examined the structure of Nb_5C_3, with two isomers presented.[33] One isomer had all three C atoms

bound to three Nb faces of the trigonal bipyramid Nb_5 cluster, which all contain a common axial Nb atom. This structure can also be considered as a substituted $2 \times 2 \times 2$ Nb_4C_4 nanocrystal, where one C atom is substituted with a Nb atom. The other isomer, calculated to be ~2.5 eV higher in energy, had the C atoms binding across all three Nb butterfly motifs of the ideal oblate trigonal bipyramid Nb_5 cluster, demonstrating that binding across all three Nb butterfly motifs is unfavourable. In this study the substituted $2 \times 2 \times 2$ cubic isomer **IV A** [$^2A_1$, C_{3v}] is also found to be the lowest in energy. With the SDD basis set all other isomers are found to be > 2 eV higher in energy (see ESI†).

Several energetically competitive isomers are found for Nb_5C_4 with the SDD basis set, with the lowest four examined with the extended basis set. Two of the isomers are generated by binding all C atoms to separate Nb faces of the trigonal bipyramid Nb_5 cluster. The lowest energy isomer, **V A** [$^2A'$, C_s], has C atoms bound to all three of the available Nb faces which share a common axial Nb atom, with the last C atom bound to one of the three remaining available Nb faces which contain the second axial Nb atom. **V D** [^2A, C_2] is the fourth lowest energy isomer (ΔE = +0.650 eV) and has the C atoms bound to two of the three available Nb faces on each side on the Nb_5 cluster, which contain opposite axial Nb atoms. The respective pairs of two C atoms are arranged so that one C atom of each set is bound to Nb faces next to one another. Isomers **V B** and **V C** have the Nb_5 cluster in the oblate trigonal bipyramid geometry. In **V C** [$^2A_1$, C_{2v}] C atoms are bound across each of the two Nb butterfly motifs with the remaining two C atoms bound to the two available outer Nb faces. Isomer **V B** [$^2A''$, C_s] can be generated from **V C** by one of the Nb butterfly motifs becoming closed while the other Nb butterfly motif opens, by a distortion of the common equatorial Nb atom. This results in the C atom bound across the open Nb butterfly motif now being bound to one of the inner Nb faces of the butterfly motif. **V B** can also be thought of as a Nb atom being bound above a C corner of a $2 \times 2 \times 2$ Nb_4C_4 nanocrystal. Isomers **V B** and **V C** are the second and third lowest energy isomers of Nb_5C_4 with a ΔE of +0.132 eV and +0.493 eV, respectively.

Four isomers of Nb_5C_5 are examined with the extended basis set. The lowest energy isomer **VI A** [$^2A'$, C_s] has a C_2 unit and C atom bound across the two Nb butterfly motifs of the oblate trigonal bipyramid Nb_5 cluster, with the remaining two C atoms bound to the two outer Nb faces. Isomer **VI B** [$^2A'$, C_s] has the five C atoms bound to all but one of the available Nb faces of the trigonal bipyramid Nb_5 cluster and is 0.333 eV higher in energy. Next is isomer **VI C** [^2A, C_1], 0.392 eV higher in energy, which has the Nb_5 cluster in the oblate trigonal bipyramid geometry with a C atom bound across the one of the Nb butterfly motifs, which is quite closed, and two C atoms bound to the two outer Nb faces. For the remaining two C atoms, one is bound to an inner Nb face of the remaining open Nb butterfly motif, while the other C atom is bound across a Nb–Nb edge on the same Nb butterfly motif. This isomer can also be considered as a $2 \times 2 \times 3$ nanocrystal fragment with a corner NbC unit removed. The final isomer is **VI D** [^2A, C_1] (ΔE = +0.599 eV), which has a C_2 unit bound across two Nb faces of the trigonal bipyramid Nb_5 cluster with C atoms bound to three of the four remaining Nb faces.

The structure of Nb_5C_6 has been examined previously by the seperate groups of Freiser and Dance.[33,35] Freiser and co-workers proposed a $2 \times 2 \times 3$ nanocrystal fragment with a C atom removed from a corner position as the structure of Nb_5C_6. Harris and Dance considered two isomers; one where C atoms are bound to all six Nb faces of the trigonal bipyramid Nb_5 cluster and another where three C_2 units are each bound across two Nb faces of the same type of Nb_5 cluster. They found the former isomer to be ~1 eV lower in energy. In the current study the lowest energy isomer **VII A** [$^2A_1$, C_{2v}] has the Nb_5 cluster in the oblate trigonal bipyramid geometry. Two acetylide C_2 units are bound across the two Nb butterfly motifs with the remaining two C atoms bound to the two outer Nb faces. In isomer **VII B** [$^2B_1$, C_{2v}] the Nb_5 cluster is in the trigonal bipyramid geometry with an actylide C_2 unit bound across two of the Nb faces, with C atoms bound to the remaining Nb faces. **VII B** is considerably higher in energy (ΔE of +1.112 eV) than **VII A**. With the SDD basis set the two isomers of Nb_5C_6 proposed by the respective groups of Freiser and Dance are found to be much higher in energy (> 1.4 eV) than the global minimum, with the former slightly the lower in energy.

C Comparison between experimental and calculated IPs

Ionisation transitions are considered for the lowest energy isomer, as well as the low-lying isomers presented, for each cluster species. The adiabatic IPs are calculated as the difference in energy between the lowest electronic states of the neutral and cation, *for the same isomer*, which can be accessed following the $\Delta S = \pm 1/2$ selection rule for ionisation. The experimental and calculated IPs are listed for the Nb_5C_y (y = 0–6) clusters in Table 1. Note that although ionisation energies both excluding and including zero point energies (ZPE) are listed in the table, only the latter numbers will be considered for discussion.

It is seen that the absolute calculated IPs for all the Nb_5C_y isomers are higher than the experimental values. In our previous investigations of the Nb_3C_y and Nb_4C_y clusters, the B3P86 method combined with the SDD/aug-cc-pVTZ basis set was also observed to systematically overestimate the experimental IPs of these metal–carbide clusters.[9] Since this study is concerned with the IP following sequential addition of C atoms, we only consider the change in IP relative to the bare Nb_5 cluster and apply a linear offset of –0.263 eV to the calculated IP values so that the experimental and calculated IPs of Nb_5 coincide. This offset value, hereafter denoted as IP*, is the value shown in the final column of Table 1. Shown in Fig. 6 are the calculated IP*s of the isomers (△) for each Nb_5C_y cluster, as well as the experimental IP (▲).

For Nb_5C, the two isomers **II A** and **II B** both have calculated IP*s in good agreement with the experimental value (deviations of +0.233 and +0.138 eV, respectively), so the experimental IP is assigned to the lowest energy isomer (**II A**). This is not a definitive assignment though as **II B** is only slightly higher in energy (ΔE = +0.072 eV).

The experimental IP of Nb_5C_2 is quite low. The two Nb_5C_2 isomers **III A** and **III B** are calculated to be quite close in energy (ΔE = +0.118) but exhibit quite different calculated IP*s. The lowest energy isomer **III A** has an IP* only 0.132 eV higher than the experimental value. Conversely, isomer **III B**

Table 1 List of experimental ionisation potentials (reported in eV) observed for Nb_5C_y (y = 0–6) clusters. Also listed are calculated transitions and ionisation potentials: excluding ZPE, including ZPE, and offset IP (*i.e.* IP*)

Cluster	Expt. IP	Isomer	Calc. transition	Calc. IP (exc. ZPE)	Calc. IP (inc. ZPE)	Calc. IP*
Nb_5	**5.45**	I A	$^3A_1 \leftarrow {}^2B_1$	5.713	5.713	5.450
Nb_5C	**5.32**	II A	$^1A \leftarrow {}^2A$	5.812	5.818	5.555
		II B	$^3B_2 \leftarrow {}^2A_1$	5.725	5.721	5.458
Nb_5C_2	**4.59**	III A	$^1A_1 \leftarrow {}^2B_1$	4.974	4.985	4.722
		III B	$^3A'' \leftarrow {}^2A'$	5.825	5.824	5.561
Nb_5C_3	**4.57**	IV A	$^1A_1 \leftarrow {}^2A_1$	5.041	5.056	4.793
Nb_5C_4	**4.97**	V A	$^3A' \leftarrow {}^2A'$	5.738	5.749	5.486
		V B	$^3A'' \leftarrow {}^2A''$	5.558	5.564	5.301
		V C	$^1A_1 \leftarrow {}^2A_1$	5.107	5.130	4.867
		V D	$^1A \leftarrow {}^2A$	5.394	5.395	5.132
Nb_5C_5	**5.01**	VI A	$^1A' \leftarrow {}^2A'$	5.376	5.388	5.125
		VI B	$^1A' \leftarrow {}^2A'$	5.378	5.403	5.140
		VI C	$^1A \leftarrow {}^2A$	5.823	5.833	5.570
		VI D	$^1A \leftarrow {}^2A$	5.565	5.587	5.324
Nb_5C_6	**5.06**	VII A	$^1A_1 \leftarrow {}^2A_1$	5.469	5.492	5.229
		VII B	$^1A_1 \leftarrow {}^2B_1$	5.852	5.870	5.607

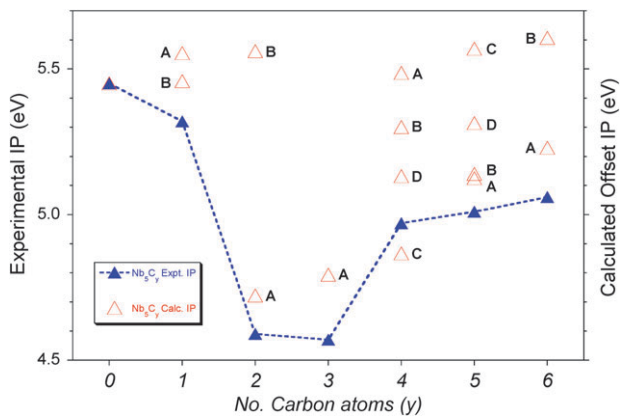

Fig. 6 Graph showing experimental IP values for the Nb_5C_y clusters as a function of y. Also shown on the same scale are the offset values, IP*, calculated using DFT. The letters (A, B, *etc*) denote the isomers for that particular cluster (see text for details).

has a much higher IP*, with a deviation of +0.971 eV relative to the experimental IP. Therefore, the experimental IP is assigned to **III A**. No definitive second ionisation onset in the Nb_5C_2 PIE spectrum is observed.

For Nb_5C_3 only one isomer is examined with the extended basis set (**IV A**), as all isomers with the SDD basis set are much higher in energy (> 2 eV). The calculated IP* of **IV A** is in good agreement with the experimental IP, with a deviation of +0.223 eV. Also the calculated IR vibrational spectrum of **IV A** is in good agreement with the experimental IR-REMPI spectrum of Nb_5C_3 (see section III.D).

The IP*s of four isomers for Nb_5C_4 are considered. The lowest energy isomer, **V A**, has a deviation of +0.516 eV between its calculated IP* and the experimental IP, which is on the borderline between what is considered to be an acceptable deviation. Of the remaining three isomers, **V C** has the smallest deviation between the calculated IP* and experimental value (−0.103 eV). However, as the calculated IP*s of the isomers assigned to Nb_5C, Nb_5C_2 and Nb_5C_3 all still overestimate the experimental IPs, the IP* of **V C** is not consistent with this trend. Furthermore, the experimental IP of Nb_5C_4 is very similar to those of Nb_5C_5 and Nb_5C_6, which is not held for Nb_5C_4 **V C** in comparison to the IP*s of the isomers assigned to the onsets of Nb_5C_5 and Nb_5C_6 (see below). The remaining two isomers, **V B** and **V D**, both have calculated IP*s in good agreement with the experimental IP, with deviations of +0.331 and +0.162 eV, respectively. However, as **V B** is much lower in energy than **V D** (ΔE = +0.132 and +0.650 eV, respectively), the former is assigned to the experimental IP. This is not a definitive assignment as despite the IP* of **V B** being in good agreement with the experimental value and having a low ΔE, isomers **V A** and **V D** cannot be totally discounted.

The four Nb_5C_5 isomers **VI A**, **VI B**, **VI C** and **VI D** have deviations between the calculated IP*s and the experimental IP of +0.115 eV, +0.130 eV, +0.560 and +0.314, respectively. Isomer **VI C** is discounted due to its large deviation. The calculated IP*s of **VI A** and **VI B** are in excellent agreement with the experimental valve, while **VI D** is in reasonable agreement. However, isomer **VI A** is assigned to the experimental IP as it is 0.333 eV lower in energy relative to **VI B**. This assignment is an interesting result, as **VI A** contains a molecular C_2 unit.

For Nb_5C_6 the deviation between the calculated IP*s and experimental IP for the isomers **VII A** and **VII B** are +0.169 and +0.547 eV, respectively. As the IP* of **VII A** is in much better agreement with the experimental value and is calculated to be significantly the lowest energy isomer by 1.112 eV, it is assigned to the observed ionisation onset. Notably, isomer **VII A** contains two molecular C_2 units.

D Comparison to previous spectroscopic data

Yang and Hackett recorded the PFI-ZEKE spectrum of Nb_5C_2, which showed a small number of bands separated by

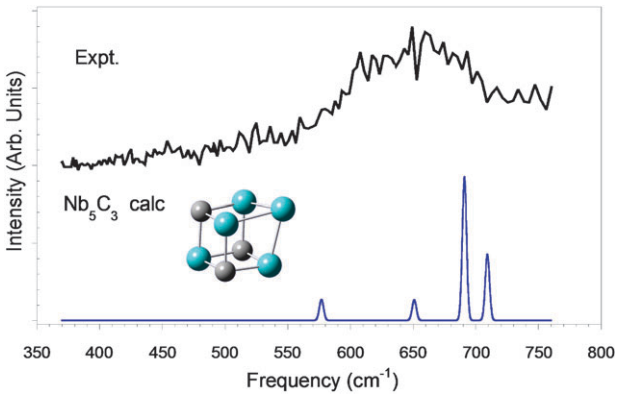

Fig. 7 Calculated IR spectrum (FWHM = 4 cm^{-1}) for Nb_5C_3 (lower trace). The upper trace shows the IR-REMPI spectrum of Nb_5C_3, reproduced with permission from ref. 23.

9 cm^{-1}, with the first band assigned to the 0–0 transition. The other bands were believed to be sequence structure as the band intensities varied with the cluster source temperature. However, no calculations were performed on the isomeric structures of Nb_5C_2. As the calculated IP* of the lowest energy isomer in this study (Nb_5C_2 **III A**) is in excellent agreement with the IP from the PFI-ZEKE and present PIE studies, it is proposed that this isomer is that for which the PFI-ZEKE spectrum was recorded. Examination of the calculated geometries (see ESI†) indeed shows no significant structural change upon ionisation, in agreement with the lack of vibrational progression observed. As this previous study was conducted utilising a liquid nitrogen cooled cluster source, there is a greater probability that the PFI-ZEKE spectrum results from the lowest energy isomer. This suggests that the extended basis set calculations for Nb_5C_2 are accurate in predicting the ordering of the **III A** and **III B** isomers, whereas the SDD basis set has the **III B** isomer lower in energy.

The IR-REMPI spectrum of Nb_5C_3 has been recorded previously and displays a single broad vibrational absorption band centred at 660 cm^{-1}.[23] Although spectra obtained in single photon IR absorption experiments are not identical to those obtained in IR-REMPI experiments (*e.g.* intensities of modes can be different due to differing vibrational anharmonicity and internal vibrational redistribution rates), they have been shown to be similar.[36]

Fig. 7 shows the experimental and our DFT-calculated IR spectra for Nb_5C_3 (between 370 and 760 cm^{-1} with no scaling) for the substituted 2 × 2 × 2 cubic isomer (**IV A**). The two most intense modes (*e* and a_1 in C_{3v}) are observed at 691 and 709 cm^{-1}. These Nb–C absorption bands are in good agreement with the maximum of the IR-REMPI spectrum. This isomer is also in good agreement with the experimental IP of Nb_5C_3.

E Onset of carbon–carbon bonding

In the growth patterns of niobium–carbide clusters, Nb_xC_y, it is important to know at what point during sequential carbon addition do the bonding arrangements change, *i.e.* when does C–C bonding become favourable in addition to Nb–C bonding.

In the Nb_3C_y cluster series, C–C bonding was found to be energetically stable for Nb_3C_y clusters when $y \geq 4$, as a very low-lying isomer containing a C_2 unit was assigned to the experimental IP.[9] In the Nb_4C_y cluster series, C–C bonding was found to occur when $y \geq 5$, with the lowest energy isomers for Nb_4C_5 and Nb_4C_6 containing one and two C_2 units substituted for C atoms in the Nb_4C_4 nanocrystal, respectively.[9] Therefore, for both the Nb_3C_y and Nb_4C_y series the onset of C–C bonding occurs when the number of C atoms is greater than the number of Nb atoms (*i.e.* $y > x$).

The C–C bonding onset point is different in the Nb_5C_y cluster series, where it is observed to occur when $y \geq 5$ (*i.e.* $y \geq x$); the lowest energy isomers for Nb_5C_5 and Nb_5C_6 contain one and two C_2 units, respectively. This onset is quite surprising as there are still free Nb faces available on the trigonal bipyramid Nb_5 cluster for C atoms to bind to. This is unlike the situation in the Nb_4C_y series, where geometrically there are no more free Nb faces available on the tetrahedral Nb_4 cluster after Nb_4C_4. The reasoning for this different onset in the Nb_5C_y series is unclear, although it appears to be related to the degree of oxidation that the Nb_5 cluster is willing to undergo, as a single C atom (formally C^{4-}) will oxidise the cluster more than an acetylide C_2 unit (formally C_2^{2-}). Indeed, analysis of the total sum of charges on the Nb atoms in the two lowest energy isomers of Nb_5C_5 shows that the isomer containing a C_2 unit has a lower charge (+3.65 in **VI A**, Fig. 8a) than the isomer containing only Nb–C bonding (+3.85 in **VI B**, Fig. 8b). This extent of total charge on the Nb atoms due to oxidation seem to be favourable for the Nb_5 cluster, as the lowest energy isomer of Nb_5C_6 (which has two C_2 units) has a similar charge (+3.87, see ESI†) to the two Nb_5C_5 isomers. Additionally, the Nb butterfly motifs available in the oblate trigonal bipyramid Nb_5 cluster can totally satisfy the bonding requirements of an acetylide C_2 unit (two σ- and two π-interactions), whereas the Nb faces on the tetrahedral Nb_4 cluster cannot (one σ- and two π-interactions).

Both the structures of Nb_5C_5 and Nb_5C_6 can be considered as a Nb atom attached to the lowest energy isomers of Nb_4C_5 and Nb_4C_6, respectively. In our previous study of the Nb_4C_y clusters the ionisation onsets of Nb_4C_5 and Nb_4C_6 were assigned to originate from meta-stable triplet states of the

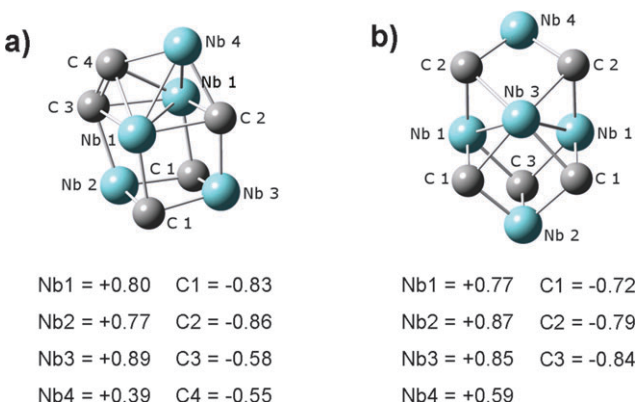

Fig. 8 The two lowest energy isomers of Nb_5C_5 (**VI A** and **VI B**) showing the atomic charges on each atom.

lowest energy isomers, with the ionisation transitions from the ground singlet states calculated to be above our highest achievable photon energy. Therefore, the structural assignments made here to Nb_5C_5 and Nb_5C_6 add further evidence towards the structures assigned for Nb_4C_5 and Nb_4C_6, respectively.

IV. Conclusion

In summary, we have determined the IPs of the Nb_5C_y (y = 0–6) clusters by photo-ionisation efficiency experiments. In conjunction with the experimental studies, the lowest energy isomers for each cluster were calculated by DFT. By comparison between the experimental IPs with those calculated for the candidate isomers, the structures of the niobium–carbide clusters could be inferred. Determination of the experimental IP was found to be critical in allowing a structural assignment to be made for Nb_5C_2, where two isomers had relative energy differences quite smaller than the expected accuracy of the DFT calculations ($\sim$0.5 eV), but had sufficiently different calculated IPs.

From the structures of the Nb_5C_y isomers assigned to the ionisation onsets, it is seen that the underlying Nb_5 cluster has two competing geometries in these clusters; either a ''prolate'' or ''oblate'' trigonal bipyramid geometry. The structures of Nb_5C and Nb_5C_3 contained Nb_5 in the former geometry, while Nb_5C_2, Nb_5C_4, Nb_5C_5 and Nb_5C_6 contained Nb_5 in the latter geometry.

Interesting results were found for the isomers assigned to the ionisation onsets of Nb_5C_5 and Nb_5C_6. For these clusters the structures contained carbon–carbon bonding in the form of C_2 units bound across the niobium butterfly motifs of the oblate trigonal bipyramid Nb_5 geometry. Previous IR-REMPI studies on various M_8C_{12} species have provided evidence of C_2 units; *e.g.* Nb_8C_{12} has an absorption resonance at 1250 cm^{-1}.[36,37] This technique could be applied to the clusters mentioned above to provide evidence of the proposed C_2 units. Alternatively, the IR-MPD technique could be applied, which has been successful for rare gas complexes of neutral bare metal clusters.[32,38,39] IR-MPD provides a higher resolution than IR-REMPI and is applicable to clusters which do not undergo thermionic emission. Furthermore, IR-MPD could help elucidate the structure of certain clusters where distinguishing between two energetically close isomers was not possible on the basis of their calculated IPs alone and the assignment was made to the lower energy isomer (*i.e.* Nb_5C, Nb_5C_4 and Nb_5C_5).

Interestingly, the structure of the Nb_5C_6 cluster contains a combination of bonding motifs from both the extensively studied Met-car (M_8C_{12}) and nanocrystal (*e.g.* M_4C_4 and $M_{14}C_{13}$) species.[16] Nb_5C_6 contains two C_2 units which are bound in environments essentially the same to which they are found in the Met-car isomer. In other words, there are two types of niobium atoms; those only involved in σ bonding with the C_2 units or those only involved in π bonding with the C_2 units. The remaining two carbon atoms are bound in environments essentially the same as in the Nb_4C_4 nanocrystal; *i.e.* carbon atoms bound to niobium faces. It would be interesting to examine how the interplay of these two bonding motifs affects the chemical properties of Nb_5C_6.

Acknowledgements

Financial support from the University of Adelaide's Faculty of Sciences is gratefully acknowledged. Support from the Australian Research Council for the purchase and maintenance of our lasers is also acknowledged. Computing resources provided by the Australian Partnership for Advanced Computing (APAC) and South Australian Partnership for Advanced Computing (SAPAC) are also gratefully acknowledged.

References

1 L.-S. Wang and C. Hansong, *Phys. Rev. Lett.*, 1997, **78**, 2983.
2 P. Liu, J. A. Rodriguez, H. Hou and J. T. Muckerman, *J. Chem. Phys.*, 2003, **118**, 7737.
3 P. Liu and J. A. Rodriguez, *J. Chem. Phys.*, 2003, **119**, 10895.
4 P. Liu, J. A. Rodriguez and J. T. Muckerman, *J. Phys. Chem. B*, 2004, **108**, 15662.
5 P. Liu, J. A. Rodriguez and J. T. Muckerman, *J. Phys. Chem. B*, 2004, **108**, 18796.
6 Y. Zhao, A. C. Dillion, Y. H. Kim, M. J. Heben and S. B. Zhang, *Chem. Phys. Lett.*, 2006, **425**, 273.
7 N. Akman, E. Durgun, T. Yildirim and S. Ciraci, *J. Phys.: Condens. Matter*, 2006, **18**, 9509.
8 V. Dryza, M. A. Addicoat, J. R. Gascooke, M. A. Buntine and G. F. Metha, *J. Phys. Chem. A*, 2005, **109**, 11180.
9 V. Dryza, M. A. Addicoat, J. R. Gascooke, M. A. Buntine and G. F. Metha, *J. Phys. Chem. A*, 2008, **112**, 5582.
10 H. Sakurai and A. W. Castleman, Jr, *J. Phys. Chem. A*, 1998, **102**, 10486.
11 J. Munoz, C. Pujol, C. Bo, J.-M. Poblet, M.-M. Rohmer and M. Benard, *J. Phys. Chem. A*, 1997, **101**, 8345.
12 L.-S. Wang, X.-B. Wang, H. Wu and H. Cheng, *J. Am. Chem. Soc.*, 1998, **120**, 6556.
13 J. Munoz, M.-M. Rohmer, M. Benard, C. Bo and J.-M. Poblet, *J. Phys. Chem. A*, 1999, **103**, 4762.
14 K. L. Knappenberger, C. E. Jones, Jr, M. A. Sobhy, I. Iordanov, J. Sofo and A. W. Castleman, Jr, *J. Phys. Chem. A*, 2006, **110**, 12814.
15 K. L. Knappenberger, P. A. Clayborne, J. U. Reveles, M. A. Sobhy, C. E. Jones, Jr, U. U. Gupta, S. N. Khanna, I. Iordanov, J. Sofo and A. W. Castleman, Jr, *ACS Nano*, 2007, **1**, 319.
16 M.-M. Rohmer, M. Benard and J.-M. Poblet, *Chem. Rev.*, 2000, **100**, 495.
17 K. Miyajima, N. Fukushima and F. Mafune, *J. Phys. Chem. A*, 2008, **112**, 5774.
18 S. Wei, B. C. Guo, H. T. Deng, K. P. Kerns, J. Purnell, S. Buzza and A. W. Castleman, Jr, *J. Am. Chem. Soc.*, 1994, **116**, 4475.
19 J. Zhao, B. Liu, H. Zhai, R. Zhou, G. Ni and Z. Xu, *Solid State Commun.*, 2002, **124**, 253.
20 J. S. Pilgrim, L. R. Brock and M. A. Duncan, *J. Phys. Chem.*, 1995, **99**, 544.
21 D.-S. Yang, M. Z. Zgierski, A. Berces, P. A. Hackett, P. N. Roy, A. Martinez, T. Carrington, Jr, D. R. Salahub, R. Fournier, T. Pang and C. Chen, *J. Chem. Phys.*, 1996, **105**, 10663.
22 D.-S. Yang and P. A. Hackett, *J. Electron Spectrosc. Relat. Phenom.*, 2000, **106**, 153.
23 D. van Heijnsbergen, A. Fielicke, G. Meijer and G. von Helden, *Phys. Rev. Lett.*, 2002, **89**, 013401.
24 C. Oshima, R. Souda, M. Aono, S. Ontani and Y. Ishizawa, *Phys. Rev. Lett.*, 1986, **56**, 240.
25 M. J. T. Frisch, G. W, H. B. Schlegel, G. E. Scuseria, M. A. Robb, J. R. Cheeseman, J. A. Montgomery Jr, T. Vreven, K. N. Kudin, J. C. Burant, J. M. Millam, S. S. Iyengar, J. Tomasi, V. Barone, B. Mennucci, M. Cossi, G. Scalmani, N. Rega, G. A. Petersson, H. Nakatsuji, M. Hada, M. Ehara, K. Toyota, R. Fukuda, J. Hasegawa, M. Ishida, T. Nakajima, Y. Honda, O. Kitao, H. Nakai, M. Klene, X. Li, J. E. Knox, H. P. Hratchian, J. B. Cross, V. Bakken, C. Adamo, J. Jaramillo, R. Gomperts, R. E. Stratmann, O. Yazyev, A. J. Austin, R. Cammi, C. Pomelli, J. W. Ochterski, P. Y. Ayala, K. Morokuma, G. A. Voth,

P. Salvador, J. J. Dannenberg, V. G. Zakrzewski, S. Dapprich, A. D. Daniels, M. C. Strain, O. Farkas, D. K. Malick, A. D. Rabuck, K. Raghavachari, J. B. Foresman, J. V. Ortiz, Q. Cui, A. G. Baboul, S. Clifford, J. Cioslowski, B. B. Stefanov, G. Liu, A. Liashenko, P. Piskorz, I. Komaromi, R. L. Martin, D. J. Fox, T. Keith, M. A. Al-Laham, C. Y. Peng, A. Nanayakkara, M. Challacombe, P. M. W. Gill, B. Johnson, W. Chen, M. W. Wong, C. Gonzalez and J. A. Pople, *GAUSSIAN 03 (Revision D. 01)*, Gaussian, Inc., Wallingford, CT, 2004.

26 E. D. Glendening, A. E. Reed, J. E. Carpenter and F. Weinhold, NBO Version 3.1.

27 S.-G. He, Y. Xie, F. Dong and E. R. Bernstein, *J. Chem. Phys.*, 2006, **125**, 164306.

28 M. B. Knickelbein and S. Yang, *J. Chem. Phys.*, 1990, **93**, 5760.

29 K. Athanassenas, D. Kreisle, B. A. Collings, D. M. Rayner and P. A. Hackett, *Chem. Phys. Lett.*, 1993, **213**, 105.

30 D. Majumdar and K. Balasubramanian, *J. Chem. Phys.*, 2004, **121**, 4014.

31 D. Majumdar and K. Balasubramanian, *J. Chem. Phys.*, 2001, **115**, 885.

32 A. Fielicke, C. Ratsch, G. von Helden and G. Meijer, *J. Chem. Phys.*, 2007, **127**, 234306.

33 H. Harris and I. Dance, *J. Phys. Chem. A*, 2001, **105**, 3340.

34 J. M. Parnis, E. Escobar-Caberra, M. G. K. Thompson, J. P. Jacular, R. D. Lafleur, A. Guevara-Garcia, A. Martinez and D. M. Rayner, *J. Phys. Chem. A*, 2005, **109**, 7046.

35 Y. G. Byun, S. Z. Kan, S. A. Lee, Y. H. Kim, M. M, R. E. Bleil, S. Kais and B. S. Freiser, *J. Phys. Chem.*, 1996, **100**, 6336.

36 G. von Helden, D. van Heijnsbergen and G. Meijer, *J. Phys. Chem. A*, 2003, **107**, 1671.

37 D. van Heijnsbergen, G. von Helden, M. A. Duncan, A. J. A. van Roji and G. Meijer, *Phys. Rev. Lett.*, 1999, **83**, 4983.

38 A. Fielicke, C. Ratsch, G. von Helden and G. Meijer, *J. Chem. Phys.*, 2005, **122**, 91105.

39 A. Fielicke, I. Rabin and G. Meijer, *J. Phys. Chem. A*, 2006, **110**, 8060.

